Check for updates

Earth-abundant and environment friendly organic–inorganic hybrid tetrachloroferrate salt $CH_3NH_3FeCl_4$: structure, adsorption properties and photoelectric behavior†

Jie Yin,* Shaozhen Shi, Jiazhen Wei, Guohang He, Lin Fan, Junxue Guo, Kaixuan Zhang, Wenli Xu, Cang Yuan, Yunying Wang, Liwen Wang, Xipeng Pu [ID] Wenzhi Li, Dafeng Zhang, Jie Wang, Xiaozhen Ren, Huiyan Ma, Xin Shao and Huawei Zhou [ID] *

Organic–inorganic hybrid-based lead perovskites show inherent and unavoidable problems such as structural instability and toxicity. Therefore, developing low-cost and environment-friendly organic–inorganic hybrid materials is extremely urgent. In this study, we prepared earth-abundant and environment-friendly organic–inorganic hybrid tetrachloroferrate salt $CH_3NH_3FeCl_4$ ($MAFeCl_4$) for optoelectronic applications. The single crystal diffraction data are assigned to the orthorhombic $MAFeCl_4$ (*Pnma* space group), with parameters $a = 11.453$ (5) Å, $b = 7.332$ (3) Å, $c = 10.107$ (5) Å, $\alpha = 90.000$, $\beta = 90.000$, and $\gamma = 90.000$. The band gap of $MAFeCl_4$ is approximately 2.15 eV. Moreover, three-emission luminescence (398, 432 and 664 nm) was observed. To the best of our knowledge, this is the first study involving the investigation of the structure, adsorption properties and photoelectric behavior of $MAFeCl_4$. A low cost photodetector based on the $MAFeCl_4$ thin film is efficient under different monochromatic light from 330 nm to 410 nm with different chopping frequencies (1.33 Hz to 40 Hz). The photoelectric conversion efficiency based on $FTO/TiO_2/MAFeCl_4$/carbon electrode device reaches 0.054% ($V_{oc} = 319$ mV, $J_{sc} = 0.375$ mA cm^{-2}, and fill factor = 0.45) under AM1.5, 100 mW cm^{-2} simulated illumination. Our findings will attract attention from the magnetic, piezoelectric and photoelectronic research fields.

Introduction

As one type of organic–inorganic hybrid material (OIHM), organic–inorganic hybrid perovskite (OIHP) has received widespread attention in the scientific community and in the industrial world. Among OIHPs, organic–inorganic hybrid lead perovskite exhibits very advantageous performances in photovoltaics,[1] lasers,[2] photodetectors[3] and so on. Recently, it has been reported that the power conversion efficiency (PCE) of solid thin film solar cells using organic-inorganic hybrid lead perovskite as a light absorbing material is up to 22%,[4] suggesting that they could become promising commercial solar cells. In addition, the preparation of perovskite by solvothermal methods greatly reduces the cost of mass production. It is well known that a high-quality photoelectric device not only requires

high performance and low cost, but also should have good stability and be environmentally friendly. However, there are some unavoidable problems in organic–inorganic hybrid lead perovskites. On the one hand, the cost of lead halide is high. On the other hand, the toxicity of lead in organic–inorganic hybrid lead perovskites is troubling.[5] Therefore, developing low-cost and environment-friendly organic–inorganic hybrid materials is extremely urgent. Recently, Pb-free and IVA-metal (Tin or Germanium)-based OIHPs have been studied. Organic-inorganic hybrid tin materials were synthesized using different halide sources to directly synthesize the nanostructure or by applying a postsynthetic anion exchange reaction.[6] Organic–inorganic hybrid germanium materials, $AGeI_3$ (A = Cs, organic cation), with second harmonic generation (SHG) properties were synthesized by replacing the inorganic cation in the A position of the perovskite unit.[7] Non-IVA-metal [single metal(+2) or mixed metal(+1, +3)]-based OIHP have also been developed. The organic–inorganic hybrid double-perovskite structure material $Cs_2AgBiBr_6$ with a long room-temperature fundamental photoluminescence (PL) lifetime was formed by incorporating nontoxic Bi^{3+} into the perovskite lattice.[8] Layered $(CH_3NH_3)_2MnCl_4$ (MA_2MnCl_4) and amorphous manganese

College of Materials Science and Engineering, Liaocheng University; School of Chemistry and Chemical Engineering, Liaocheng University, Shandong Provincial Key Laboratory of Chemical Energy Storage and Novel Cell Technology, Liaocheng 252059, China. E-mail: yinjieily@163.com; zhouhuaweiopv@163.com

† Electronic supplementary information (ESI) available. CCDC 1585495. For ESI and crystallographic data in CIF or other electronic format see DOI: 10.1039/c8ra03498b

$MAMnI_3$ were exploited for optoelectronic applications.[9,10] A lead-free highly stable $C_6H_4NH_2CuBr_2I$ compound that exhibits extraordinary hydrophobic behaviour was developed.[11] However, the efficiency and cost of the abovementioned materials are not ideal, and the stability is not very good.

Therefore, it is very necessary to develop new types of low-cost and environment-friendly organic–inorganic hybrid materials. In this study, we prepared $CH_3NH_3FeCl_4$ (MAFeCl$_4$) single crystals and films (see Experiment section). The crystal structure, luminescence, band gap, adsorption properties and photoelectric behavior were studied.

Experimental

Preparation of CH₃NH₃FeCl₄ single crystal

162.5 mg FeCl$_3$ and 67.5 mg CH$_3$NH$_3$Cl were added to a mixed solvent (3 mL methanol, 3 mL ethanol and 2 mL 35–36% HCl). The above solution was heated to 80 °C for 2 h. Then, the temperature was reduced to 40 °C over 20 h, following which a yellow-brown single crystal was obtained.

Single crystal X-ray diffraction (XRD) characterization

Data were collected on a Bruker SMART CCD diffractometer using Mo Kα radiation ($\lambda = 0.71073$ Å). The structures were solved by direct methods and expanded *via* difference Fourier techniques with the SHELXL-97 program.

Preparation of the CH₃NH₃FeCl₄ optoelectronic device

Patterned FTO-coated glass substrates with sheet resistances of 15 Ω sq^{-1} were coated with a TiO$_2$ compact layer by spin-coating the TiO$_2$ organic sol at 3000 rpm for 30 s, followed by drying at 450 °C for 30 min following our previous literature report.[9,10] The MAFeCl$_4$ layer was prepared by spin coating 162.5 mg of FeCl$_3$ and 67.5 mg of the CH$_3$NH$_3$Cl mixed precursor at 3000 rpm for 30 s, followed by gradual heating to 70 °C; the layer was baked at this temperature for 30 min. Finally, the carbon electrodes were prepared following our previous literature protocol;[9,10] the MAFeCl$_4$ layer was coated with conductive-carbon paste by the doctor-blade method using adhesive tapes for creating patterns and spaces, followed by drying at 70 °C for 40 min. The size of the FTO/TiO$_2$/MAFeCl$_4$/carbon electrode device was 1 cm^2.
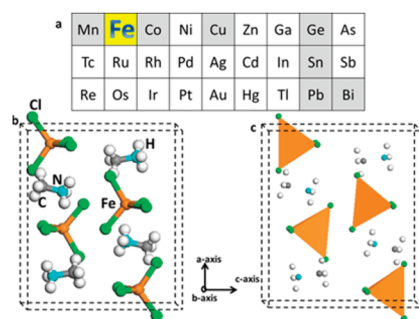

Fig. 1 (a) The position of iron in the periodic table of elements. (b and c) Schematic diagrams of the unit cell structure in ball-stick type and polyhedron type, respectively.

Table 1 Crystal data and structure refinement for CH₃NH₃FeCl₄

Compound	C·H₆·Cl₄·Fe·N
Chemical composition	$CH_3NH_3FeCl_4$
Crystal system	Orthorhombic
Space group, Z	*Pnma*
Temperature/K	298(2) K
a, Å	11.453(5)
b, Å	7.332(3)
c, Å	10.107(5)
α, deg	90
β, deg	90
γ, deg	90
Volume, Å³	848.7(7)
ρ, Mg m^{-3}	4, 1.798
μ, mm^{-1}	2.939
Total reflections, R(int)	3945/810, 0.0370
Data/restraints/parameters	810/0/42
Final R_1, wR_2 [$I > 2\gamma(I)$]	$R_1 = 0.0393$, w$R_2 = 0.0971$

Characterization of the CH₃NH₃FeCl₄ optoelectronic device

Nanostructures of MAFeCl$_4$ films were characterized by scanning electron microscopy (SEM, Hitachi SEM S-4800). UV-vis absorption spectra and diffuse reflectance spectra were obtained using a UV-vis-NIR spectrometer (PerkinElmer, λ, 750S). The photocurrent–time performance of FTO/TiO$_2$/MAFeCl$_4$/carbon electrode devices was studied using an electrochemical workstation system (CHI760, Chenhua, and Shanghai) equipped with a solar simulator (IV5, PV Measurements, Inc., United States). The photocurrent–time with incident photon (wavelength) and frequency response was measured by an electrochemical workstation system (CHI760, Chenhua, and Shanghai) equipped with a quantum efficiency/spectral response (SR)/incident photon to current conversion efficiency (IPCE) measurement system (QEX10, PV Measurements, Inc., United States). The photocurrents of the devices were measured under a bias voltage of 0.00 V.

Results and discussion

The color of the MAFeCl$_4$ single crystal is yellow-brown. The single crystal structure was solved by a direct method and was

Table 2 Bond lengths [Å] and angles [deg] for CH₃NH₃FeCl₄^a

Bond or angles	Lengths or [deg]
Fe(1)–Cl(3)	2.162(2)
Fe(1)–Cl(2)	2.181(2)
Fe(1)–Cl(1)	2.1857(15)
Fe(1)–Cl(1)#1	2.1857(15)
N(1)–C(1)	1.397(9)
Cl(3)–Fe(1)–Cl(2)	110.82(11)
Cl(3)–Fe(1)–Cl(1)	110.28(6)
Cl(2)–Fe(1)–Cl(1)	108.16(5)
Cl(3)–Fe(1)-Cl(1)#1	110.28(6)
Cl(2)–Fe(1)–Cl(1)#1	108.16(6)
Cl(1)–Fe(1)–Cl(1)#1	109.07(9)

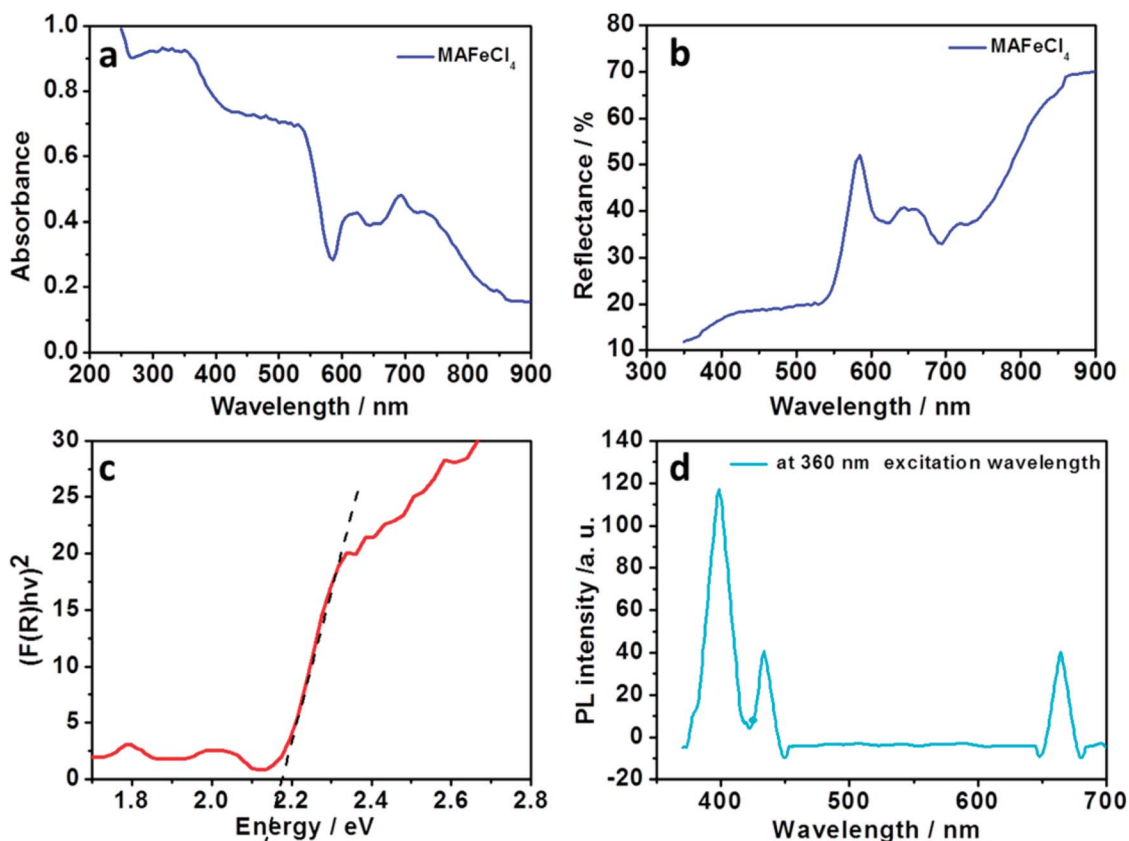^{a} Symmetry transformations used to generate equivalent atoms: #1 x, $-y + 3/2$, z.

Fig. 2 (a–c) UV-Vis absorption spectrum, diffuse reflection spectrum and Kubelka–Munk spectrum of MAFeCl$_4$, respectively; (d) photoluminescence spectrum of MAFeCl$_4$ at 360 nm excitation wavelength.

extended using the SHELXL-97 program using differential Fourier technology. The single crystal diffraction data were assigned to the orthorhombic MAFeCl$_4$ (*Pnma* space group), with parameters $a = 11.453$ (5) Å, $b = 7.332$ (3) Å, $c = 10.107$ (5) Å, $\alpha = 90.000$, $\beta = 90.000$, and $\gamma = 90.000$. The schematic diagram of the unit cell structure is shown in Fig. 1. As seen from the projection down to the *ac*-plane (Fig. 1), tetrachloroferrate FeCl$_4^-$ ions are distributed in the unit cell. Due to the four Cl ligands and the d^5 of Fe^{3+}, FeCl$_4^-$ ions form regular tetrahedron structures. Thus, there should be a residual electron on the remaining d-orbit. MA$^+$ is distributed around the FeCl$_4^-$ ions. There is a relatively short hydrogen bond (NH···Cl, 2.797 Å) between the MA$^+$ groups and the FeCl$_4^-$ ions. Accordingly, the shortest Cl···Cl distances between the neighboring FeCl$_4^-$ ions is 4.133 Å, which is much longer than the van der Waals distance (3.90 Å). These structural features suggest stronger s–d interactions between the FeCl$_4^-$ ions and the MA$^+$ groups. The detailed crystal data and structural refinement of the MAFeCl$_4$ single crystal can be observed in Tables 1, 2, S1, and S2.† The structure of the MAFeCl$_4$ single crystal is different from that of the classical perovskite structure (ABX$_3$). First, the crystal structure of MAFeCl$_4$ is no longer the perovskite structure. Second, the valence of Fe in MAFeCl$_4$ is +3, which is different from that of Pb in MAPbI$_3$. Third, the band gap of MAFeCl$_4$ is different from that of MAPbI$_3$. Thus, the

performance of the MAFeCl$_4$ single crystal is also different from that of the classic perovskite.

In order to characterize the absorbance properties of MAFeCl$_4$, UV-Vis absorption spectra were recorded. The UV-Vis absorption spectrum of MAFeCl$_4$ is shown in Fig. 2a. Strong absorption from 300 nm to 568 nm is observed. The absorbance of MAFeCl$_4$ declined steeply from 539 nm to 582 nm, indicating the presence of the band gap. In order to characterize the reflection property of MAFeCl$_4$, diffuse reflection spectroscopy was performed. The diffuse reflection spectrum of MAFeCl$_4$ is shown in Fig. 2b. The reflectivity of MAFeCl$_4$ decreases from 351 nm to 530 nm. The above results are consistent with the characteristics of the UV-visible absorption of MAFeCl$_4$. In order to acquire the band gap of MAFeCl$_4$, the diffuse reflectance spectrum was converted into the Kubelka–Munk spectrum (Fig. 2c). According to the Kubelka–Munk formula, $F(R) = (1 - R)^2/2R$, where R represents the percentage of reflection, the relationship of the incident photon energy ($h\nu$) and E_g can be expressed as the transformed Kubelka–Munk relation, $[F(R)h\nu]^p = A(h\nu - E_g)$, where E_g is the band gap energy, A is the absorption constant, h is the Planck 's constant, ν is the frequency of the light (s^{-1}) and P is the power index that is related to the optical absorption process. Theoretically, P is equal to 1/2 or 2 for an indirect or a direct allowed transition, respectively. The E_g of MAFeCl$_4$ was determined to be approximately 2.15 eV from the intercept of the linear plot on the *X* axis
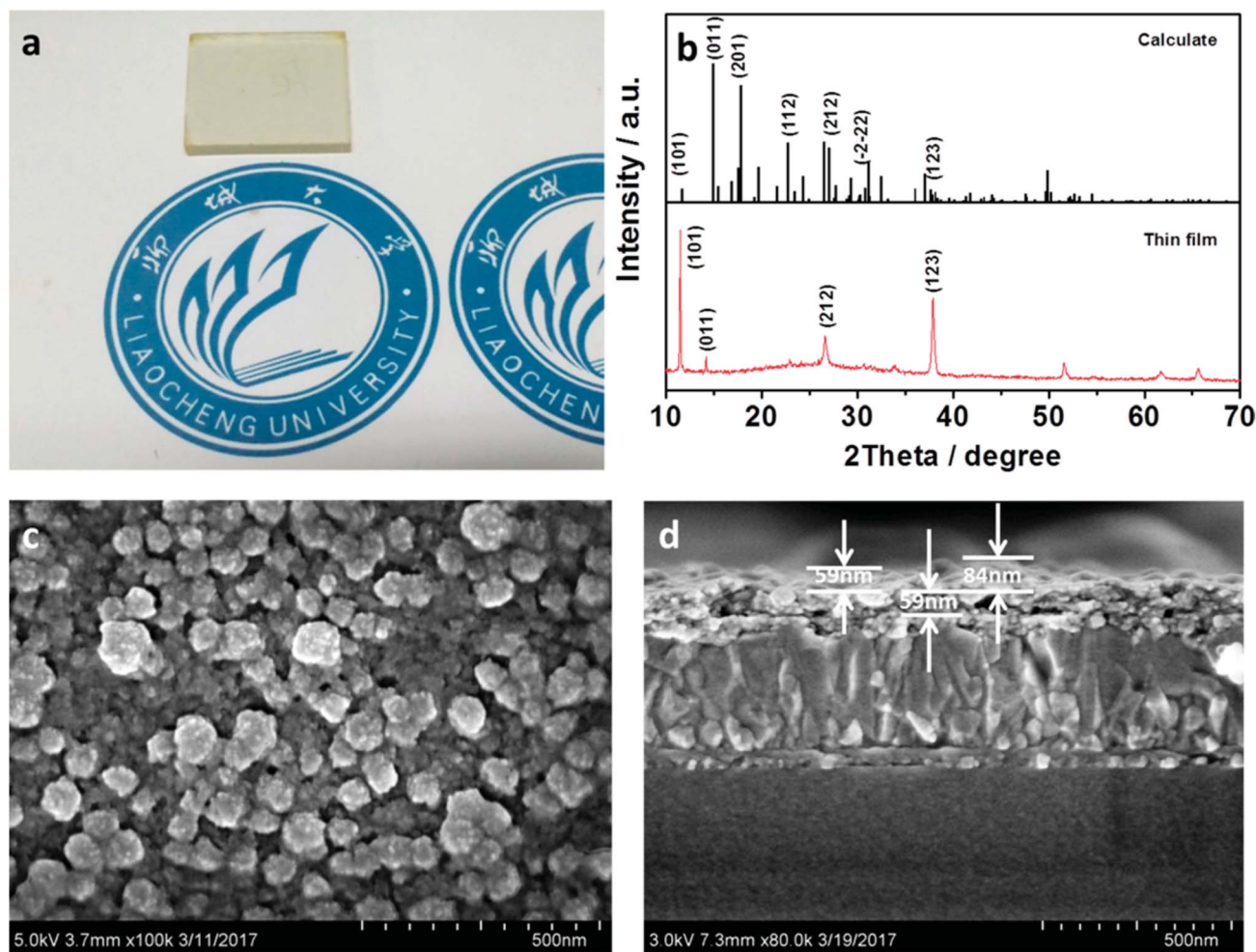
Fig. 3 (a) Picture of the MAFeCl$_4$ thin film on the TiO$_2$ layer. (b) Calculated powder XRD profiles from the MAFeCl$_4$ single crystal and the MAFeCl$_4$ thin film on the TiO$_2$ layer. (c) SEM images of MAFeCl$_4$ on the TiO$_2$ layer. (d) Amplifying cross-sectional SEM images of the MAFeCl$_4$ device. (FTO/TiO$_2$/MAFeCl$_4$).

if MAFeCl$_4$ is regarded as a directly allowed transition. After UV-Vis absorption spectroscopy and diffuse reflection spectroscopy for MAFeCl$_4$ were performed, the photoluminescence (PL) spectroscopy of MAFeCl$_4$ was also carried out. The PL spectrum of MAFeCl$_4$ is shown in Fig. 2d. The emission peaks at 398, 432 and 664 nm are observed at 360 nm excitation wavelength. Thus, the PL characteristic of MAFeCl$_4$ is attributed to these three emission peaks. MAFeCl$_4$ thin films (Fig. 3a) were prepared by spin-coating a mixture of equimolar MACl and FeCl$_3$ in DMF solution.

In order to determine the structure of the film, we recorded the XRD profiles of the MAFeCl$_4$ thin film. The diffraction XRD results of the MAFeCl$_4$ thin film on TiO$_2$ are shown in Fig. 3b. The diffraction peaks of MAFeCl$_4$ films on TiO$_2$ were basically consistent with the diffraction peaks calculated from the MAFeCl$_4$ single crystal. The corresponding crystal faces of each diffraction peak are shown in Fig. 3b. Strong peaks at 11.48°, 14.18°, 26.62°, and 37.91° are assigned to the (101), (011), (212), and (123) planes, respectively. In terms of the intensity of the peaks, the intensity of (101) peak was clearly stronger than that

of the other peaks. These results suggest that the surface of the TiO$_2$ electron collecting layer induces the growth of MAFeCl$_4$ along the (101) plane. In order to study the morphology of the MAFeCl$_4$ thin film, we carried out surface SEM analysis. The SEM test result is shown in Fig. 3c. It can be clearly seen that non-uniform-size nanoparticles were formed on the surface of the TiO$_2$ layer. The sizes of the nanoparticles are about 50 to 90 nm. In order to test the uniformity and thickness of the FTO/TiO$_2$/MAFeCl$_4$ device, we tested the cross-sectional SEM image. The result is shown in Fig. 3d. The MAFeCl$_4$ thin film is uniformly covered on the TiO$_2$ film. The thickness of the MAFeCl$_4$ film ranges from 59 nm to 84 nm. In addition, the thickness of the electron collection layer (TiO$_2$) is uniform (about 59 nm).

The photoresponse of MAFeCl$_4$ has not been studied. Thus, photoresponsive devices based on MAFeCl$_4$ were fabricated. We prepared a carbon electrode as the back electrode on the MAFeCl$_4$ thin film by a doctor-blade, and evaluated the photoresponse by recording the photocurrent density–time characteristics. The I$_{ON}$/I$_{OFF}$ photocurrent density response of the

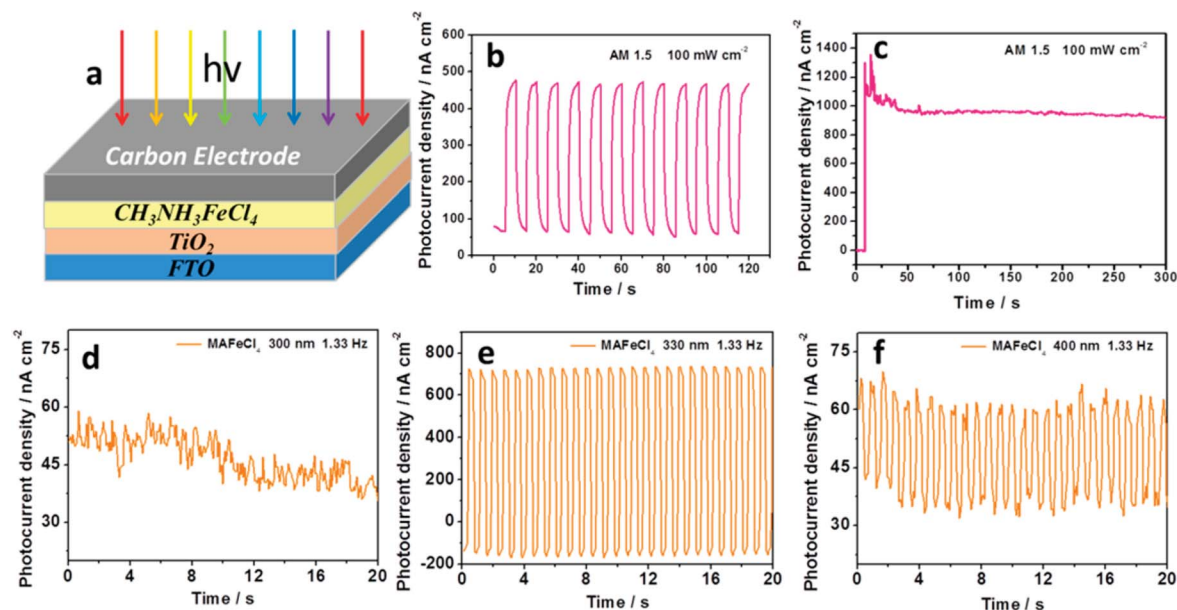Fig. 4 (a) Schematics of the FTO/TiO$_2$/MAFeCl$_4$/carbon electrode device. (b) Photocurrent density–time characteristics of the FTO/TiO$_2$/MAFeCl$_4$/carbon electrode device under on/off illumination of AM 1.5 (100 mW cm^{-2}) using a solar simulator. (c) Photocurrent density–time characteristics of the FTO/TiO$_2$/MAFeCl$_4$/carbon electrode device under continuous illumination of AM 1.5 (100 mW cm^{-2}) using a solar simulator. (d–f) Photocurrent density–time characteristics of the FTO/TiO$_2$/MAFeCl$_4$/carbon electrode device under different wavelengths (300, 330 and 400 nm, respectively) with a flashlight frequency of 1.33 Hz.

MAFeCl$_4$ device is clearly observed under ON/OFF illumination of AM 1.5 (100 mW cm^{-2}) using a solar simulator (Fig. 4b). As time progressed, the photocurrent density increased. In order to determine the time required for the photocurrent density could attain stability, the photocurrent density–time characteristics of the FTO/TiO$_2$/MAFeCl$_4$/carbon electrode device were investigated under continuous illumination of AM 1.5 (100 mW cm^{-2}) using a solar simulator (Fig. 4c). An evident photoresponse with maximum photocurrent density of 1352 nA cm^{-2} at 14.4 seconds was observed. The photocurrent density can stabilize after 54 seconds of illumination. In order to investigate the monochromatic photocurrent-response of the MAFeCl$_4$ device, the monochromatic photocurrent response at different wavelengths with a flash frequency of 1.33 Hz was measured. The results are shown in Fig. 4. The I$_{ON}$/I$_{OFF}$ photocurrent density response of the MAFeCl$_4$ device is not observed at 300 nm (Fig. 4d). At a wavelength of 330 nm, the I$_{ON}$/I$_{OFF}$ photocurrent density response is significantly enhanced (Fig. 4e). The I$_{ON}$/I$_{OFF}$ photocurrent response is also observed at a wavelength of 400 nm (Fig. 4f). At 410 nm, the I$_{ON}$/I$_{OFF}$ photocurrent response is significantly weaker, but still measurable (Fig. S1†). At 430 nm and 450 nm, the I$_{ON}$/I$_{OFF}$ photocurrent response was ineffective (Fig. S2 and S3†). The reason for this ineffective I$_{ON}$/I$_{OFF}$ photocurrent response from 400 to 558 nm might be due to the unreasonable device structure or the energy level mismatch. In the future, we will optimize the device structure and energy level of the HTM material to generate I$_{ON}$/I$_{OFF}$ photocurrent responses from 400 to 558 nm. The photoelectric conversion efficiency based on the FTO/TiO$_2$/MAFeCl$_4$/carbon electrode device reaches 0.054% (V_{oc} = 319 mV, J_{sc} = 0.375 mA cm^{-2}, and

fill factor = 0.45) under AM1.5, 100 mW cm^{-2} simulated illumination (Fig. S4 and Table S3†).

The frequency of the writing-light is significant for the efficiency of an optical-logic device. The photoelectric responses of the MAFeCl$_4$ device were investigated under 330 nm illumination with different chopping-frequencies (1.33 Hz, 40 Hz, 60 Hz, and 80 Hz). The results are shown in Fig. S5.† The best photoelectric response of the MAFeCl$_4$ device is obtained at 1.33 Hz (Fig. S5a†). A stable photoelectric response is also observed at 40 Hz and 60 Hz (Fig. S5b and S5c†), which becomes weaker at 80 Hz (Fig. S5d†). Thus, the photocurrent–density response device is ineffective at 80 Hz. The effective photocurrent-response of the MAFeCl$_4$ device at high frequencies was probed to enhance the efficiency of the MAFeCl$_4$ optical-logic device. Our findings will be of interest in the magnetic, piezoelectric and photoelectronic research fields.

Conclusions

We prepared earth-abundant and environmentally friendly organic–inorganic CH$_3$NH$_3$FeCl$_4$ (MAFeCl$_4$) and studied its crystal structure, luminescence, band gap, adsorption properties and photoelectric behavior. The band gap of the orthorhombic MAFeCl$_4$ was determined to be approximately 2.15 eV. A low cost photodetector based on the MAFeCl$_4$ thin film is efficient under different monochromatic light ranging from 330 nm to 410 nm with different chopping frequencies (1.33 Hz to 40 Hz). Although the photoelectric conversion efficiency (0.054%) based on the FTO/TiO$_2$/MAFeCl$_4$/carbon electrode device is low, there will be significant room for improvement.

Conflicts of interest

There are no conflicts to declare.

Acknowledgements

Notes and references

1 H.-S. Kim, C.-R. Lee, J.-H. Im, K.-B. Lee, T. Moehl, A. Marchioro, S.-J. Moon, R. Humphry-Baker, J.-H. Yum, J. E. Moser, M. Graetzel and N.-G. Park, Lead Iodide Perovskite Sensitized All-Solid-State Submicron Thin Film Mesoscopic Solar Cell with Efficiency Exceeding 9%, *Sci. Rep.*, 2012, **2**, 591.

2 H. Zhu, Y. Fu, F. Meng, X. Wu, Z. Gong, Q. Ding, M. V. Gustafsson, M. T. Trinh, S. Jin and X. Y. Zhu, Lead halide perovskite nanowire lasers with low lasing thresholds and high quality factors, *Nat. Mater.*, 2015, **14**(6), 636–U115.

3 L. Dou, Y. Yang, J. You, Z. Hong, W.-H. Chang and G. Li, Solution-processed hybrid perovskite photodetectors with high detectivity, *Nat. Commun.*, 2014, **5**, 5404.

4 W. S. Yang, B. W. Park, E. H. Jung, N. J. Jeon, Y. C. Kim, D. U. Lee, S. S. Shin, J. Seo, E. K. Kim, J. H. Noh and S. I. Seok, Iodide management in formamidinium-lead-halide-based perovskite layers for efficient solar cells, *Science*, 2017, **356**(6345), 1376–1379.

5 B. Brun and P. Pouillart, Chemotherapy of metastatic breast cancer, *Bull. Cancer*, 2000, **87**(9), 643–653.

6 T. C. Jellicoe, J. M. Richter, H. F. J. Glass, M. Tabachnyk, R. Brady, S. E. Dutton, A. Rao, R. H. Friend, D. Credgington, N. C. Greenham and M. L. Boehm, Synthesis and Optical Properties of Lead-Free Cesium Tin Halide Perovskite Nanocrystals, *J. Am. Chem. Soc.*, 2016, **138**(9), 2941–2944.

7 C. C. Stoumpos, L. Frazer, D. J. Clark, Y. S. Kim, S. H. Rhim, A. J. Freeman, J. B. Ketterson, J. I. Jang and M. G. Kanatzidis, Hybrid Germanium Iodide Perovskite Semiconductors: Active Lone Pairs, Structural Distortions, Direct and Indirect Energy Gaps, and Strong Nonlinear Optical Properties, *J. Am. Chem. Soc.*, 2015, **137**(21), 6804–6819.

8 A. H. Slavney, T. Hu, A. M. Lindenberg and H. I. Karunadasa, A Bismuth-Halide Double Perovskite with Long Carrier Recombination Lifetime for Photovoltaic Applications, *J. Am. Chem. Soc.*, 2016, **138**(7), 2138–2141.

9 Z. H. Nie, J. Yin, H. W. Zhou, N. Chai, B. L. Chen, Y. T. Zhang, K. G. Qu, G. D. Shen, H. Y. Ma, Y. C. Li, J. S. Zhao and X. X. Zhang, Layered and Pb-Free Organic-Inorganic Perovskite Materials for Ultraviolet Photoresponse: (010)-Oriented $(CH_3NH_3)(2)MnCl_4$ Thin Film, *ACS Appl. Mater. Interfaces*, 2016, **8**(41), 28187–28193.

10 X. Zhang, J. Yin, Z. Nie, Q. Zhang, N. Sui, B. Chen, Y. Zhang, K. Qu, J. Zhao and H. Zhou, Lead-free and amorphous organic–inorganic hybrid materials for photovoltaic applications: mesoscopic $CH_3NH_3MnI_3/TiO_2$ heterojunction, *RSC Adv.*, 2017, **7**(59), 37419–37425.

11 X. Li, X. Zhong, Y. Hu, B. Li, Y. Sheng, Y. Zhang, C. Weng, M. Feng, H. Han and J. Wang, Organic–Inorganic Copper(II)-Based Material: A Low-Toxic, Highly Stable Light Absorber for Photovoltaic Application, *J. Phys. Chem. Lett.*, 2017, **8**(8), 1804–1809.